

## Test-Particle Transport in Strong Electrostatic Drift Turbulence with Finite Larmor Radius Effects

G. Manfredi and R. O. Dendy

United Kingdom Atomic Energy Authority, Government Division, Fusion, Culham, Abingdon, OX14 3DB, United Kingdom  
(Received 12 February 1996)

Test-particle transport arising from  $\mathbf{E} \times \mathbf{B}$  motion in a turbulent plasma is investigated numerically. The electrostatic field is determined by solving the Hasegawa-Mima model for two-dimensional drift turbulence. In the linear regime the particles experience stochastic diffusion, but in the fully nonlinear, strongly turbulent regime the diffusion rate is greatly reduced. Finite Larmor radius effects, relevant to alpha-particle transport in tokamaks, are also shown to strongly inhibit the level of transport. [S0031-9007(96)00339-0]

PACS numbers: 52.25.Fi, 52.35.Ra, 52.65.-y

Studies of the transport of energetic alpha particles offer a new opportunity to investigate the nature of plasma turbulence in tokamaks. Because the Larmor radii of alpha particles born in fusion reactions greatly exceed those of the majority ions, the response of alpha particles to a turbulent field in the plasma differs from that of the thermal ions. For example, the larger scale of gyromotion and drift motion will smooth out the effects of short wavelength turbulence, creating a differential response for particles of different energies. Given a theoretical understanding of this differential effect, observations of alpha-particle transport may yield information on the characteristics of the turbulence.

The role of turbulence in tokamak plasma transport has been widely investigated [1–3]. Transport due to drift turbulence remains an area of particular interest: it involves low frequency, electrostatic waves and is dominated by the  $\mathbf{E} \times \mathbf{B}$  drift [1–4]. There is, for example, increasing evidence of a good fit between observations of transport in the core region of tokamaks and large-scale gyrofluid and gyrokinetic simulations of transport arising from ion-temperature-gradient driven turbulence [5–9]. Meanwhile, initial measurements [10] show broadly classical confinement of fusion alpha particles in the Tokamak Fusion Test Reactor.

In this numerical study, we quantify two key aspects of this problem, namely the impact of large scale turbulent structures and of finite Larmor radius (FLR) on the transport of test particles. Previous studies have shown that a field composed of linear drift waves can induce stochastic diffusion of test particles [11–15]. Here, we compute the field self-consistently by adopting a long-established model for drift turbulence, the Hasegawa-Mima equation [4]:

$$\frac{\partial}{\partial t} (\phi - \nabla^2 \phi) - [\nabla \phi \times \mathbf{e}_z \cdot \nabla] \nabla^2 \phi = \frac{\partial \phi}{\partial x}. \quad (1)$$

This equation describes 2D drift turbulence in the plane perpendicular to the magnetic field direction  $\mathbf{e}_z$ , and can be derived from the ion continuity equation with  $\mathbf{E} \times \mathbf{B}$  and polarization drifts, and assuming an adiabatic re-

sponse for the electrons. Time is normalized to  $L_n/C_s$  ( $C_s = \sqrt{T_e/m_i}$  is the sound speed), space to the thermal Larmor radius  $\rho_s = C_s \Omega_i^{-1}$  ( $\Omega_i = eB/m_i$ ), and the potential to  $(T_e/e)\rho_s/L_n$ .  $L_n$  is a typical scale of variation of the equilibrium density profile. The generalized vorticity  $W = \phi - \nabla^2 \phi$  is the actual quantity transported by the flow. The computational box is periodic in the  $x$  direction ( $0 < x < L_x$ ) and finite in  $y$  ( $-L_y < y < L_y$ ; both  $\phi$  and  $W$  vanish at  $y = \pm L_y$ ). A dissipative term, of the form  $\nu \nabla^2 W$ , is added to the right hand side of Eq. (1) to control the numerical noise at small wavelengths, although no forcing is included at this stage (freely decaying turbulence). The test particles follow the  $\mathbf{E} \times \mathbf{B}$  drift:  $d\mathbf{r}/dt = \mathbf{B} \times \nabla \phi / B^2$ . Although in the (purely adiabatic) Hasegawa-Mima model the flux of thermal bulk ions is zero, the test particles can still experience stochastic diffusion.

First, we consider the linearized version of Eq. (1), which describes uncoupled drift waves obeying the (dimensionless) dispersion relation  $\omega = k_x / (1 + k^2)$ . The initial condition is a random vorticity distribution

$$W(x, y, t = 0) = \sum_n \sum_m \frac{1}{(n^2 + m^2)^{1/2}} \times \sin\left[\frac{\pi}{2L_y} m(y - L_y)\right] \times \cos\left(\frac{2\pi}{L_x} nx + \beta_{mn}\right), \quad (2)$$

where  $\beta_{mn}$  are random phases. This choice corresponds to a spectrum  $|\phi_k| \propto k^{-3}$ ,  $k = \sqrt{m^2 + n^2}$ . A typical realization of the initial vorticity field is shown in Fig. 1. In the present example the sums in Eq. (2) are in the ranges  $2 \leq m \leq 8$ ,  $1 \leq n \leq 8$ , with  $L_x = 2L_y = 20\rho_s$  and  $\nu = 0.002\rho_s^3\Omega_i/L_n$ . We take a relatively large viscosity because we shall eventually compare the results with those obtained in the nonlinear regime, which requires some dissipation in order to control the numerical noise. The test particles are initially located in a narrow band around  $y = 0$ . After following the trajectories of

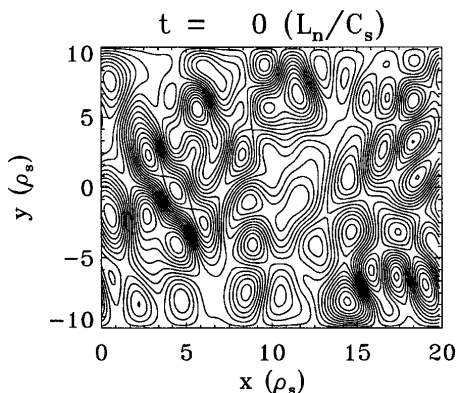


FIG. 1. Typical vorticity field from the superposition of 56 waves.

4000 particles, we compute several statistical quantities. In particular, the mean square displacement  $Y^2(t)$ , the diffusion coefficient in the  $y$  (nonperiodic) direction  $D_y(t)$ , and the kurtosis  $K(t)$  are

$$D_y(t) = \frac{Y^2(t)}{2t} = \frac{\langle [y(t) - y(0)]^2 \rangle}{2t},$$

$$K(t) = \frac{\langle [y(t) - y(0)]^4 \rangle}{3\langle [y(t) - y(0)]^2 \rangle^2}, \quad (3)$$

where the angular brackets denote an average over all particles and  $K = 1$  for a Gaussian distribution. For a truly diffusive process, the diffusion coefficient should be asymptotically time independent. The time history of  $Y^2(t)$  is shown in Fig. 2(a), and displays a linear growth corresponding to a diffusion coefficient (normalized to gyro Bohm)  $D_y \approx 0.01D_{gB}$ , where  $D_{gB} = \rho_s^3 \Omega_i / L_n$ . The kurtosis rapidly approaches unity, as expected. The distribution of the 4000 test particles (Fig. 3) closely approximates a Gaussian, although it is not perfectly symmetric.

We now solve the fully nonlinear Hasegawa-Mima equation (1) with the same parameters as before. This

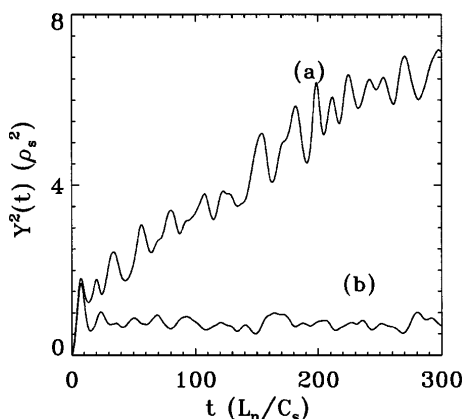


FIG. 2. Time history of the mean square test-particle displacement in the case of freely decaying turbulence (no forcing): (a) linear regime, (b) nonlinear regime.

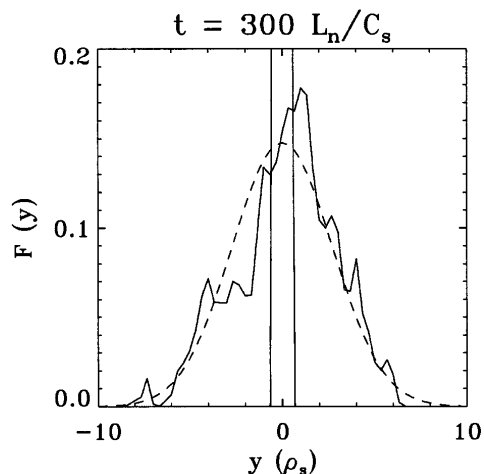


FIG. 3. Normalized distribution of the test particles at the end of the linear evolution (solid line). The broken line represents a Gaussian distribution of the same width. The vertical lines indicate the initial distribution of the particles.

virtually suppresses test-particle diffusion, as shown by the time history of the mean square displacement  $Y^2(t)$  [Fig. 2(b)]. We attribute this effect to the large scale structures appearing at the end of the simulation (Fig. 4; compare Fig. 1), as expected from the inverse cascade [16]. These structures evolve more slowly, both linearly and nonlinearly: for large wavelengths, all waves propagate with the same phase velocity, which can be eliminated by a Galilean transformation, thus suppressing all time dependence in the potential. The nonlinear terms are also negligible when  $\rho_s^2 k^2 \ll 1$ . Therefore, particles trapped in these large vortices follow the field lines adiabatically, and are less likely to “jump” from one vortex to another; nonadiabatic motion is indeed recognized as the origin of stochastic diffusion [11]. The test-particle statistics are still Gaussian, as indicated by the kurtosis ( $K \approx 1$ ) and by the particle distribution (Fig. 5).

Let us now consider the effect of a forcing term in Eq. (1). In practice, a source of fluctuations is always

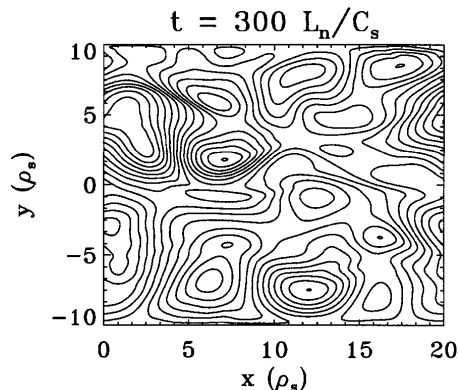


FIG. 4. Vorticity field at the end of the simulation for the nonlinear regime.

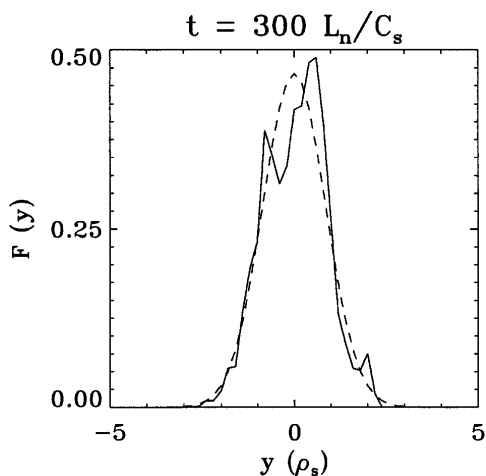


FIG. 5. Normalized distribution of test particles at the end of the nonlinear evolution (solid line). The broken line represents a Gaussian distribution of the same width.

present, whose nature depends on the linear instability responsible for wave excitation. However, it may not be easy to derive an appropriate spectrum for the forcing term: we have chosen a broad spectrum of the form  $\nu k^2 |W_k(t=0)|$  where  $W_k(t=0)$  is the initial vorticity distribution, Eq. (2). This choice has two advantages: it exactly balances the dissipation term, so that a fluctuating steady state is reached rapidly, avoiding the irrelevant transient; and, secondly, it can be used for a direct comparison with the linear regime, while a source localized on a particular wave number would not be meaningful linearly.

The random phases are updated at regular time intervals, while the viscosity is, in this case, slightly larger:  $\nu = 0.005 D_{gB}$ . The evolution of the mean square displacement in the linear and nonlinear regimes (Fig. 6) again shows a reduction in transport due to turbulent mode couplings, which is less dramatic than in the previous case (with forcing, we have measured  $D_{lin} \approx 3 D_{nonlin} \approx 0.013 D_{gB}$ ). This differential diffusion is also visible from the particle distribution in space (Fig. 7). Now the forcing and nonlinear terms are in competition: the former tries to restore the original, small-scale spectrum, while the latter favors large-scale structures. If the rate of injection at small scales is too fast, the nonlinear terms do not have time to react, and the transport will be dominated by the forcing. A crude estimate is obtained by comparing the strength of the nonlinear and forcing terms, which yields the dimensionless parameter  $A \equiv \nu(1 + k_{max}^2)$ . For the nonlinearities to dominate we need  $A \ll 1$ , and in our example  $A \approx 0.05$ .

For high energy alpha particles the above guiding-center model is not adequate, and FLR effects must be taken into consideration. If the gyration frequency is much larger than the typical rate of change of the electric field, FLR effects can be modeled numerically by

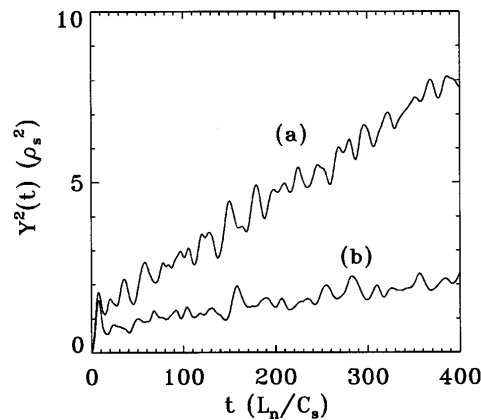


FIG. 6. Time history of the mean square displacement (case with forcing): (a) linear regime, (b) nonlinear regime.

“spreading” the particle over a ring centered at the position of its guiding center [17]. This introduces an averaging operation, which tends to suppress the smaller-scale components of the electric field (a similar effect could arise from the so-called banana orbits, induced by the inhomogeneity of the magnetic field in toroidal geometry). This point has been raised in the context of electron diffusion in a stochastic magnetic field [18]. We present the results of a linear simulation with  $L_x = 2L_y = 20\rho_s$ ,  $\nu = 5 \times 10^{-6} \rho_s^3 \Omega_i / L_n$ . The field spectrum is that described in our first simulation. Five groups of particles

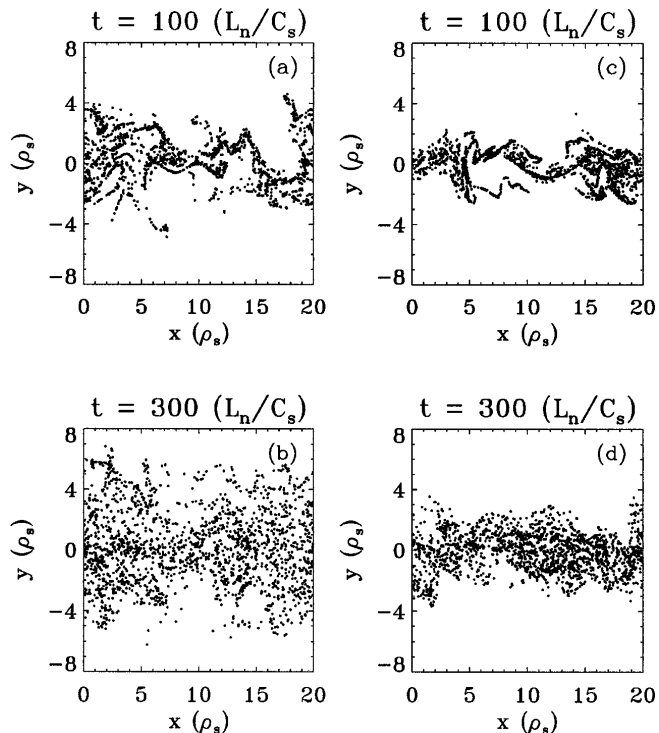


FIG. 7. Particle distribution at  $t = 100 L_n / C_s$  and  $t = 300 L_n / C_s$  for the linear (a),(b) and nonlinear (c),(d) regimes.

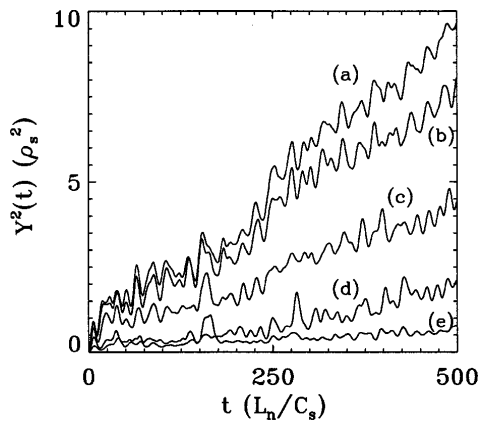


FIG. 8. Time history of the mean square displacement for five groups of test particles with Larmor radii  $\rho_i/\rho_s = 0.0$  (a), 0.3 (b), 0.6 (c), 1.0 (d), and 1.6 (e).

were followed in the same field, their Larmor radii  $\rho_i$  ranging from zero to  $1.6\rho_s$ . The mean square displacement  $Y^2(t)$  (Fig. 8) clearly demonstrates that FLR effects can strongly inhibit stochastic diffusion.

In conclusion, our study shows that the formation of large vortices in strong electrostatic turbulence results in coherent advective motion for the test particles, suppressing the stochastic diffusion which occurs in the linear limit. This result supports an early conjecture by Hasegawa, MacLennan, and Kodama [19]. Furthermore, the transport of high energy ions is greatly reduced by the averaging effect introduced by their large Larmor radius. Comparison of measured diffusion rates of alpha particles of different energies could therefore be used to infer spectral properties of the underlying turbulent field.

The authors acknowledge helpful discussions with Dr. J.W. Connor. This work was partially funded by the Commission of the European Communities (Contract No. ERBCHIBICT941009), the UK Department of Trade and Industry, and Euratom.

- 
- [1] P. C. Liewer, Nucl. Fusion **25**, 543 (1985).
  - [2] W. Horton, Phys. Rep. **192**, 1 (1990).
  - [3] J. W. Connor and H. R. Wilson, Plasma Phys. **36**, 719 (1994).
  - [4] A. Hasegawa and K. Mima, Phys. Fluids **21**, 87 (1978).
  - [5] G. W. Hammett and F. W. Perkins, Phys. Rev. Lett. **64**, 3019 (1990).
  - [6] R. D. Sydora *et al.*, Phys. Rev. Lett. **64**, 2015 (1990).
  - [7] A. W. Dimits and W. W. Lee, Phys. Fluids B **3**, 1557 (1991).
  - [8] S. E. Parker *et al.*, Phys. Plasmas **1**, 1461 (1994).
  - [9] G. Manfredi *et al.*, Phys. Plasmas **3**, 202 (1996).
  - [10] R. K. Fisher *et al.*, Phys. Rev. Lett. **75**, 846 (1995).
  - [11] R. Kleva and J. F. Drake, Phys. Fluids **27**, 1686 (1984).
  - [12] W. Horton, Plasma Phys. Controlled Fusion **27**, 937 (1985).
  - [13] W. Horton and D.-I. Choi, Plasma Phys. Controlled Fusion **29**, 901 (1987).
  - [14] M. Pettini *et al.*, Phys. Rev. A **38**, 344 (1988).
  - [15] M. Ottaviani, Europhys. Lett. **20**, 111 (1992).
  - [16] M. Ottaviani and J. A. Krommes, Phys. Rev. Lett. **69**, 2923 (1992).
  - [17] W. W. Lee, J. Comput. Phys. **72**, 243 (1987).
  - [18] H. E. Mynick and J. A. Krommes, Phys. Rev. Lett. **43**, 1506 (1979).
  - [19] A. Hasegawa, C. G. MacLennan, and Y. Kodama, Phys. Fluids **22**, 2122 (1979).